A Simple Phenology-Based Vegetation Index for Mapping Invasive Spartina Alterniflora Using Google Earth Engine

Ronglong Xu ⓘ, Siqing Zhao ⓘ, and Yinghai Ke ⓘ

Abstract—*Spartina alterniflora* (*S. alterniflora*) after introduced to China, has rapidly expanded along the coastline and become one of the top invasive plants in coastal wetland. While it has been well accepted that phenological information derived from multitemporal remotely sensed data improves vegetation mapping accuracy, previous research primarily relied on scene-based features for invasive plant mapping. In the coastal regions with frequent cloud cover such as South China coast, extracting phenological features at scene level was impossible due to lack of sufficient cloud-free imageries. In this study, we aimed to propose a simple phenological vegetation index (PVI) using pixel-level composition of Sentinel-2 observations with the assist of Google Earth Engine platform. By developing and comparing six PVIs, separability analysis showed that phenological normalized vegetation difference index (PNDVI) of *S. alterniflora* and other land cover types were more separable than other PVIs and single-season NDVI. Based on the PNDVI, we further proposed supervised and unsupervised Otsu thresholding methods for *S. alterniflora* extraction. The overall accuracies of supervised Otsu-PNDVI-thresholding method using 10-fold cross validation reached 97.84%, and that of the unsupervised Otsu-PNDVI-thresholding method reached 97.20%. Kappa Z-test statistics showed that both supervised and unsupervised Otsu-PNDVI-thresholding methods yielded statistically similar accuracies as random forest classifiers based on six PVIs, and higher accuracies than scene-based classification. The success of the unsupervised Otsu-PNDVI-thresholding method suggested that the method was practical and operational for *S. alterniflora* mapping and its expansion monitoring in wide area such as South China coast.

Index Terms—Google Earth Engine (GEE), invasive species, phenological vegetation index (PVI), phenology, Sentinel-2, *Spartina alterniflora*.

Ronglong Xu is with the College of Geospatial Information Science and Technology, Capital Normal University, Beijing 100048, China (e-mail: aa821932327@gmail.com).

Siqing Zhao is with the College of Resource Environment and Tourism, Capital Normal University, Beijing 100048, China (e-mail: zsq1616@gmail.com).

Yinghai Ke is with the Laboratory Cultivation Base of Environment Process and Digital Simulation, Beijing Laboratory of Water Resource Security, Capital Normal University, Beijing 100048, China (e-mail: yke@cnu.edu.cn).

I. INTRODUCTION

THE INVASION of nonnative plant species has posed significantly negative effects on ecosystem services as well as human wellbeing [1]–[3]. In 1979, for the purpose of consolidating seashore and mitigating the coastal erosion, *Spartina alterniflora* (*S. alterniflora*) was introduced to Chinese coastal areas [4]–[6]. Due to the strong reproductive capacity and the high tolerance to the habitat, *S. alterniflora* has undergone an extensive expansion along many regions of Chinese coastline, ranging from Guangxi Province in South China (21°33′ N, 108°08′ E) to Liaoning Province (40°20′ N, 122°35′ E) in North China [7]–[9]. Since 2003, *S. alterniflora* has been listed as top invasive plants in China by the State Environmental Protection Administration of China [10], [11]. Rapid expansion of *S. alterniflora* has threatened coastal wetland ecosystems by accelerating soil salinization, encroaching the habitats of native plants and leading to reduction of bird species [12]–[16]. This raises necessities for accurate detection and mapping of *S. alterniflora* in order to better understand the invasive mechanisms, mitigate its further invasion and impacts, and assist decision making in coastal wetland ecosystem management and restoration.

Remote sensing techniques have been widely used for invasive plant species mapping [17]–[19]. The task of invasive species mapping involves discrimination of the target species from the native species and other land cover types. In addition to spectral features, in recent years more and more studies have paid attention to the phenological information provided from multitemporal remote sensing imagery [20]–[24]. For example, Diao and Wang [20] extracted phenological metrics using the adaptive Savitzky–Golay smoothing function based on monthly Landsat imagery and then detected the invasive salt cedar in southwestern United States using random forest (RF) algorithm. Tian *et al.* [25] categorized the existing strategies incorporating phenological features into two classes, i.e., scene-based methods and pixel-based methods. Scene-based methods utilized cloud-free (or mostly cloud-free) scenes to derive phenological features, while pixel-based methods composited phenological features for each pixel using cloud-free observations among all available scenes, even if a scene was cloud contaminated. In areas with frequent cloud cover, scene-based methods are problematic because cloud clear images are not sufficient for deriving useful phenological information. Pixel-based methods can mitigate this problem by using all cloud-free observations

of a pixel through a year regardless the cloud coverage at scene level [26], [27]. Pixel-based processing is both computational and demanding, while this issue can be solved by Google Earth Engine (GEE, https://earthengine.google.com), a cloud-based platform with supercomputing capacity for massively geospatial data analysis.

Detailed literature review on invasive species mapping show that existing methods are dominated by machine learning (ML) classification algorithms [28], [29]. The mainstream classifiers include support vector machines, artificial neural networks, decision tree classification, classification and regression tree (CART), *k*-nearest neighbors, and RF [30]–[32]. Although ML classification methods generally yield good accuracies, they usually require plenty of features, such as geometry features, texture features as well as spectral features, which is complicated to operate. It is well accepted that the performances of ML-based classification are sensitive to the selection of feature sets. In addition, application of ML-based classification algorithms over large area (e.g., Southeast China Coast) requires large amount of training samples, which is time consuming and labor intensive.

Given the importance of phenological features in invasive species mapping and the advantage of GEE in efficient pixel-based phenological feature extraction, we aim to construct a simple and effective phenological vegetation index (PVI) for *S. alterniflora* mapping in cloudy and humid coastal area in southeast China. The objectives of this study are as follows.

1) Propose a PVI based on Sentinel-2 time series imagery using pixel composition method, based on which *S. alterniflora* can be distinguished from native vegetation types and its background land cover types.
2) Present a simple threshold-based method for *S. alterniflora* identification solely based on PVI.
3) Evaluate the effectiveness of PVI-threshold-based method by comparing to both pixel- and scene-based ML classification methods.

II. STUDY AREA AND DATA

A. Study Area

Our study area is located in the southeastern coastal regions of mainland China. It includes Beibu Gulf in Guangxi Province (covering two National Natural Reserves, i.e., Shankou Mangrove National Natural Reserve and Hepu Dugong National Natural Reserve) [see Fig. 1(a)], Zhangjiangkou Mangrove National Natural Reserve [see Fig. 1(b)], and Jiulongjiangkou Mangrove Provincial Natural Reserve in Fujian Province [see Fig. 1(c)]. The climate is subtropical marine monsoon climate with annual average temperature varying from 15 to 22° and annual average precipitation ranging from 1200 to 2000 mm. Port development, rapid economic growth as well as abundant habitats of microbial communities have made these sties the priorities of the coastal management program. For these sites, dominant intertidal vegetation species include invasive *S. alterniflora* and native Mangrove forests [25], [33]. In recent years, intertidal mudflats of these natural reserves have been extensively invaded by *S. alterniflora* [34], [35].
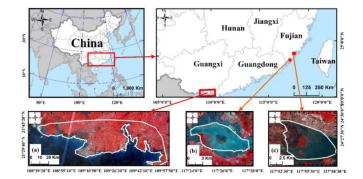

Fig. 1. Study regions situated in southeast coastal region of China. (a) Beibu Gulf in Guangxi Province. (b) Zhangjiang Estuary of Fujian Province. (c) Jiulongjiang River Estuary in Fujian Province.

TABLE I
GENERAL SKETCH OF THE SENTINEL-2 BANDS

Sentinel-2 Bands	Central Wavelength (um)	Resolution(m)
Band 1-Coastal aerosol	0.443	60
Band 2-Blue	0.490	10
Band 3-Green	0.560	10
Band 4-Red	0.665	10
Band 5-Vegetation Red Edge	0.705	20
Band 6-Vegetation Red Edge	0.740	20
Band 7-Vegetation Red Edge	0.783	20
Band 8-NIR	0.842	10
Band 8A-Vegetation Red Edge	0.865	20
Band 9-Water vapour	0.945	60
Band 10-SWIR-Cirrus	1.375	60
Band 11-SWIR	1.610	20
Band 12-SWIR	2.190	20

B. Datasets

Sentinel-2A and Sentinel-2B are two matching satellites launched by European Space Agency on June 2015 and March 2017, respectively. Detailed description of the Sentinel-2A/B multispectral instrument (MSI) sensors is provided in Table I. In order to mitigate the influence of cloud contamination and tidal inundation in the study area, we collected all available Sentinel-2A and Sentinel-2B MSI data with cloud/cirrus cover less than 70% from 2018 to 2019 on GEE platform. There were a total of 2732 images covering the three study sites, among which 1150 images had cloud cover less than 70%. Only 132 images were cloud free. Taking the Beibu Gulf in the humid and cloudy Southern China Coast as an example, only images acquired on three dates (March 22, September 30, and October 30) are cloud-free in year 2018.

Reference data were randomly sampled as evenly as possible throughout the research sites covering *S. alterniflora*, Mangrove forests, and other land cover types (hereafter named "Others"), including water and mudflat (see Fig. S1–S6 in Supplementary

Materials). With the assistance of the field survey reported in the existing literature [33], [36], the land cover type of each point was allocated by visual interpretation of very high-resolution (VHR) image with spatial resolution less than 10 m [21]. Specifically, the visual interpretation was conducted by three experienced remote sensing experts, who have visited different coastal wetlands in China and have comprehensive understanding of the phenological characteristics of *S. alterniflora* and Mangrove trees. VHR Google Earth images in year 2018 and 2019 were used for interpretation, including images collected on March 20, April 28, August 27, September 29, November 3, and November 30 in year 2018, and images collected on January 26, February 7, April 10, August 10, October 26, and November 30 in year 2019. Although not all images were available for each study site, they can help to visualize and analyze the seasonal change of vegetation greenness. The visual interpretation was also assisted by several previous studies including UAV images collected by Zhu *et al.* [24], the reference samples by Liu *et al.* [16], and Tian *et al.* [25], and the resultant maps by Li *et al.* [34] and Tian *et al.* [25]. Once the samples were interpreted by one expert, they were re-examined by other experts and all experts discussed the ones with uncertainties. All artificial land cover types such as crops and ponds were manually excluded. The reference pixels include 1867 pixels for *S. alterniflora*, 1973 for Mangrove, and 2046 for others type together for the three study sites.

III. METHODOLOGY

Fig. 2 illustrates the flow chart of the methodology. First, all Sentinel-2 datasets with cloud cover less than 70% were preprocessed by removing cloudy pixels (see Part A). Second, pixels during key phenological periods, i.e., senescence period and green period, were selected, and six PVIs were derived based on phenological composition of six commonly used vegetation indices (see Part B). Third, the optimal phenological index was selected through separability analysis (see part C), and both supervised and unsupervised threshold-based classification method were presented to extract *S. alterniflora* (see part D). Finally, the PVI-based thresholding classification methods were compared with ML classifiers at both pixel- and scene-based level, thus, to further evaluate the effectiveness of all these available classification methods (see Part E and Part F).

A. Data Preprocessing

Using 10th and 11th bits of QA60 band of Sentinel-2 data, we removed clouds and cirrus from Sentinel-2 imagery. We then analyzed the phenological characteristics of the major land cover types in the study areas. Fig. 3 demonstrates time series normalized difference vegetation index (NDVI) of three sample pixels covered by *S. alterniflora*, Mangrove, and mudflats, respectively. Note that these pixels were manually selected to ensure that sufficient valid observations were available to recover full temporal profile of NDVI time series. It is explicit that *S. alterniflora* has different phenological features from Mangrove trees. Mangrove trees are evergreen, while *S. alterniflora* are not. NDVI of Mangrove trees is consistently high throughout the year, while that of *S. alterniflora* is low from early January

Fig. 2. Overview of the processing workflow.

Fig. 3. Temporal profile of NDVI of Mangrove, *S. alterniflora* and Mudflat during 2018–2019.

to the end of April and raises maximum from June to October. From January to April, NDVI differences between Mangrove and *S. alterniflora* are large, while from June to October, NDVI differences between *S. alterniflora* and mudflat are large. Therefore, we considered the day of year (DOY) 1 to 142 belongs to senescence period, and DOY 154 to 270 belongs to green period for *S. alterniflora* [25], [43], [44].

Fig. 4 illustrates the number of valid observations (no cloud/cirrus cover) across three study sites of two key phenological periods during year 2018–2019. Valid observations over Zhangjiang Estuary and Jiulongjiang River Estuary ranged from 38 to 51 and 15 to 27 in green period, and 31 to 39, 16

Fig. 4. Spatial distributions of valid observations for all pixels in the study areas. (a) Valid observations over Beibu Gulf study area. (b) Valid observations over Zhangjiang Estuary. (c) Valid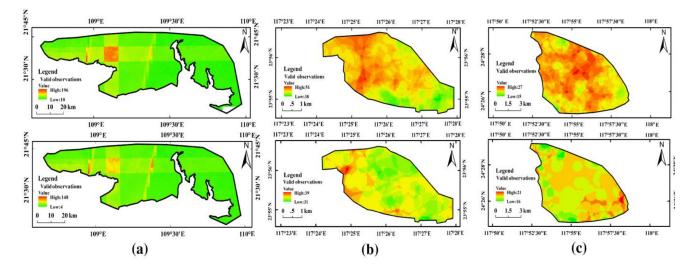 observations over Jiulongjiang River Estuary. The upper subfigure illustrates the valid observations in green period, and the bottom one illustrates valid observations in senescence period.

TABLE II
FORMULAS OF THE EXISTING VEGETATION INDICES WITH THEIR REFERENCES

Index	Equation	Reference
NDVI	$NDVI = \dfrac{NIR - Red}{NIR + Red}$	Tucker,1978 [37]
EVI	$EVI = \dfrac{2.5(NIR - Red)}{NIR + 6Red - 7.5Blue + 1}$	Huete et al.,2002 [38]
DVI	$DVI = NIR - Red$	Jordan,1969 [39]
gDVI	$gDVI = NIR - Green$	Sripada et al., 2006 [40]
gNDVI	$gNDVI = \dfrac{NIR - Green}{NIR + Green}$	Gitelson et al.,1998 [41]
SAVI	$SAVI = \dfrac{1.5(NIR - Red)}{NIR + Red + 0.5}$	Huete,A.R.,1988 [42]

to 21 in senescence period, respectively. The number of valid observations of the Beibu Gulf ranged from 10 to 196 with an average number of 38 in green period, and from 4 to 148 with an average number of 25 in senescence period.

B. Phenological Vegetation Indices

For each cloud-free pixel, we calculated NDVI, enhanced vegetation index (EVI), difference vegetation index (DVI), green difference vegetation index (gDVI), green NDVI (gNDVI), and soil-adjusted vegetation index (SAVI) using the equations in Table II.

All valid pixels acquired during DOY 1–142 were considered as senescence pixels, and those acquired during DOY 154–270 were green pixels. Therefore, for each vegetation index, we constructed two seasonal VI composite images, i.e., Senescence VIs (SeVI, including SeNDVI, SeEVI, SeDVI, SegDVI, SegNDVI, SeSAVI) and Green VIs (GrVI, including GrNDVI, GrEVI, GrDVI, GrgDVI, GrgNDVI, GrSAVI). SeVI images and GrVI images were generated as the maximum VI value on a per-pixel basis during the senescence period and during the green period,

respectively. PVIs (PNDVI, PEVI, PDVI, PgDVI, PgNDVI, PSAVI) were then calculated by using the following equation:

$$\text{CVI} = \text{GrVI} + \text{SeVI} \tag{1}$$

$$\text{PVI} = \frac{\text{CVI}}{\text{CVI}_{\max} - \text{CVI}_{\min}} \tag{2}$$

where CVI denotes composited vegetative index calculated as the sum of GrVI and SeVI derived from the candidate index; $\text{CVI}_{\max}$ and $\text{CVI}_{\min}$ denote the maximum and minimum CVI values across the CVI image, respectively.

C. Separability Analysis

Intraclass and interclass variabilities are the key measures to evaluate how well *S. alterniflora* can be separated from the other classes. Here, we adopted separability index (SI) presented by Somers *et al.* [45] to assess the spectral separability of *S. alterniflora* and other classes in terms of PVIs. SI defines the separability between a pair of class by incorporating both intraclass and interclass variability measurements. The formula is calculated as

$$\text{SI}_{sj} = \frac{\Delta\text{inter}_{sj}}{\Delta\text{intra}_{sj}} = \frac{|\overline{\mu_s} - \overline{\mu_j}|}{1.96 \times (\sigma_s + \sigma_j)} \tag{3}$$

where SI_{sj} refers to the SI between *S. alterniflora* (denoted as s) and one of the other two classes (Mangrove or Others, denoted as j). $\overline{\mu_s}$ and $\overline{\mu_j}$ denote the mean vegetation index of *S. alterniflora* and class j, respectively; σ_s and σ_j denote the standard deviation of the candidate PVI of class s and class j. $|\overline{\mu_s} - \overline{\mu_j}|$ represents the interclass variability between class s and class j, and $(\sigma_s + \sigma_j)$ represents the sum of intraclass variability of the two given classes. Greater differences between $\overline{\mu_s}$ and $\overline{\mu_j}$ and smaller within-class variances yield higher value of SI. The average value of SI between *S. alterniflora* and each of the other classes were considered as the average separability between *S. alterniflora* and non-*S. alterniflora*.

D. Classification Using Otsu Thresholding Algorithm

In this study, we adopted and compared two strategies of threshold-based classification, i.e., supervised and unsupervised strategies. Both strategies utilized Otsu thresholding algorithm to determine suitable thresholds of PVIs in order to separate *S. alterniflora* from other classes. Otsu algorithm is a nonparametric approach for automatic threshold selection proposed by Otsu *et al.* [46], which determines the optimal threshold by going through all possible thresholds and selecting the one that the intraclass variance is minimum. For the supervised classification strategy, thresholds between each pair of the classes were determined using Otsu algorithm based on the training samples. The PVI thresholds were then implemented over the entire study area (all three study regions). For the unsupervised classification strategy, multiclass Otsu thresholding algorithm was applied over the PVI images and the pixels within each study region were automatically classified into three classes, and the land cover type was assigned to each class based on its PVI range.

E. Scene- and Pixel-Based ML Classification Methods

We further compared the proposed methods with pixel-based and scene-based ML classification methods. The scene-based classification was conducted based on cloud free imagery. As the three study sites were located within different scenes, cloud free image scenes acquired on similar dates were selected. For Beibu gulf, the images include those acquired on March 9, September 30, and November 4 in 2018, and on January 23 2019; for the other two sites, the images include those acquired on March 10, September 26, November 5 in 2018, and on January 24 in 2019. The four dates represent spring, summer, autumn, and winter. For each of the images, we calculated the six vegetation indices, and implemented RF classification (hereafter called RF-spring, RF-summer, RF-autumn, and RF-winter). For the pixel-based method, we implemented RF and CART based on multiple features of vegetation indices. Based on the training datasets, each of the RF and CART was trained based on 1) 6 GrVIs, 2) 6 SeVIs, 3) 6 PVIs.

When it comes to the coefficient of the CART classifier, we utilized the default coefficient of GEE ("max Nodes" as null and "minLeafPopulation" as 1); for RF classifier, the "number of trees" was 4, and all other parameters were set as default values in GEE, i.e., "variablesPerSplit" as null, "minLeafPopulation" as 1, "bagFraction" as 0.5, "maxNodes" as null, "seed" as 0.

F. Training and Evaluation of the Classification Methods

Two strategies were used to train and evaluate the supervised Otsu thresholding method, scene-based ML methods, and pixel-based ML methods. First, ten-fold cross validation was applied to each of the classification strategies to assess the stability and reliability of the methods. Classification accuracies were evaluated using the average overall accuracies (OA), Kappa coefficient, producer's accuracies (PA), and user's accuracies (UA). Second, from the reference pixels, 70% were randomly selected from each class as training samples (see Figs. S1, S3, and S5 in Supplementary Materials), and the rest 30% were used as testing samples (Figs. S2, S4, and S6 in Supplementary
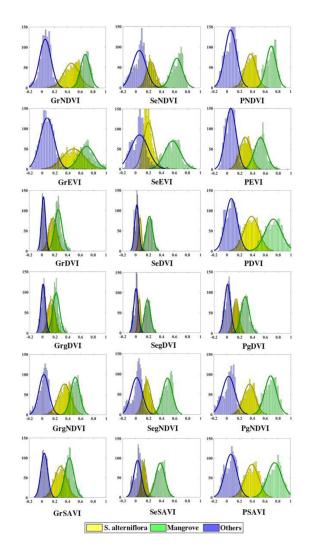

Fig. 5. Histogram of senescence vegetation indices, green vegetation indices, and phenological vegetation indices.

Materials). In addition to OA, PA, UA, and kapa coefficient, Kappa Z-test [47] was conducted in order to evaluate whether the accuracies of two different classification algorithms were statistically different. The null hypothesis of Kappa Z-test is that the Kappa values from two classification methods are equal. Z statistics can be calculated as

$$Z = \frac{k_1 - k_2}{\sqrt{(\text{Var}(k_1) + \text{Var}(k_2)}} \tag{4}$$

where k_1 and k_2 are the Kappa coefficients of the two classification algorithms; $\text{Var}(k_1)$ and $\text{Var}(k_2)$ are their variances, respectively, calculated from the confusion matrix [48]. The null hypothesis is rejected if the Z-statistic is higher than the critical value (1.96 at 95% confidence level).

IV. RESULTS

A. Separability Assessment

Fig. 5 presents the histograms of GrVIs, SeVIs, and PVIs calculated from the training samples of *S. alterniflora*, Mangrove, and "Others." From the GrVI diagrams (left column of
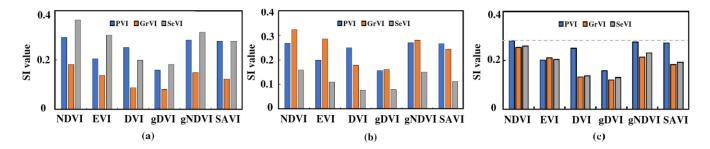
Fig. 6. SI value of the vegetation indices between different classes. (a) SI value of the vegetation indices between *S. alterniflora* and Mangrove trees. (b) SI value of the vegetation indices between *S. alterniflora* and "Others." (c) SI value of the vegetation indices between *S. alterniflora* and non-*S. alterniflora.*

Fig. 5), it is obvious that *S. alterniflora* was easy to be confused with Mangrove forest in green period, as the range of VIs of *S. alterniflora* had a large overlap with that of Mangrove trees. Whereas in senescence period (middle column of Fig. 5), the VIs of *S. alterniflora* inclined to overlap with those of "Others." Take NDVI as an example, in green period, GrNDVI of *S. alterniflora* had an overlap from 0.44 to 0.70 with that of Mangrove forest. GrNDVI of *S. alterniflora* showed almost no overlap with "Others" class. In senescence period, SeNDVI of *S. alterniflora* (ranging from 0.04 to 0.48) had little overlap with that of Mangrove trees, while it has a large overlap with "Others" (ranging from -0.2 to 0.38). PVIs, however, have greatly mitigated the histogram overlaps among the three classes (right column of Fig. 5). Compared to GrNDVI and SeNDVI, the range of PNDVI did not change significantly for Mangrove trees or "Others," while PNDVI of *S. alterniflora* moved toward the middle between those of Mangrove trees and "Others" so that the overlaps between *S. alterniflora* and each of Mangrove or "Others" greatly reduced. Likewise, PgNDVI and PSAVI also showed great mitigation of histogram overlap compared to the corresponding green period and senescence period indices. GrSAVI of *S. alterniflora* (0.01–0.52) has a large overlap with Mangrove (0.22–0.64) in green period with a range of 0.22–0.52, while in senescence period, *S. alterniflora* (0.04–0.28) has a large overlap with "Others" (-0.14–0.20) within a range of 0.04–0.20.

Among the six candidate PVIs, it can be found that PNDVI, PgNDVI, and PSAVI of the three classes were more separable than PEVI, PDVI, and PgDVI. For EVI, DVI, and gDVI, large overlaps were found in green indices between *S. alterniflora* and Mangrove trees. Although the corresponding phenological indices reduced the overlap, the confusions between *S. alterniflora* and Mangrove trees (or "Others") were still considerable.

Fig. 6 demonstrates the SI values of the GrVIs, SeVIs, and PVIs. It can be discovered that the SeVIs yielded higher SI value than PVIs and GrVIs when discriminating *S. alterniflora* from Mangrove trees (>0.198), while GrVIs had the lowest SI value (< 0.182) [see Fig. 6(a)]. In contrast, the SI values of GrVIs between *S. alterniflora* and "Others" were higher than PVIs and SeVIs [see Fig. 6(b)], suggesting that *S. alterniflora* is more separable from Mangrove trees in senescence period, while it is more separable from "Others" in green period, which is consistent with Fig. 4. Neither GrVIs nor SeVIs alone can discriminate *S. alterniflora* for they always left one type of
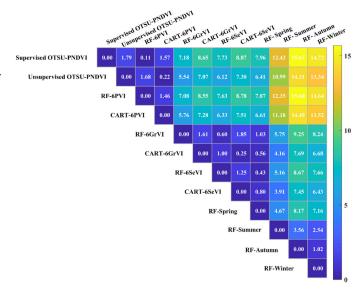

Fig. 7. Z-statistic values of the candidate classification algorithms.

land cover to be confused. Although PVIs did not produce the highest separability between *S. alterniflora* and Mangrove trees or between *S. alterniflora* and "Others," PVIs produced higher SI value between *S. alterniflora* and non-*S. alterniflora* when compared to single season derived VIs [see Fig. 6(c)], indicating that PVIs were suitable for discerning *S. alterniflora* from the other two classes.

The comparison of the six PVIs shows that PNDVI had the maximum SI value than others, whose SI value is 0.279, followed by PgNDVI with SI of 0.275 and PSAVI with SI of 0.271 [see Fig. 6(c)]. The other three indices have lower SI values. The highest SI value of PNDVI between *S. alterniflora* and non-*S. alterniflora* indicates that PNDVI produces the highest interclass separability and the lowest intraclass variability. Therefore, PNDVI was selected as the optimal phenological index to discriminate *S. alterniflora*.

B. Comparison of Classification Accuracies

Supervised and unsupervised Otsu thresholding classification approaches solely based on PNDVI (hereafter named supervised Otsu-PNDVI and unsupervised Otsu-PNDVI, respectively) were compared with the more complex RF and CART classification methods. For the supervised Otsu-PNDVI, the

TABLE III
CLASSIFICATION ACCURACIES WITH THE TEN-FOLD CROSS-VALIDATION

Classifier	PA(%)			UA(%)			OA(%)	Kappa
	Spartina	Mangrove	Others	Spartina	Mangrove	Others		
Supervised Otsu-PNDVI	95.23	99.09	99.02	98.02	98.84	96.77	97.84	0.968
Unsupervised Otsu-PNDVI	92.71	99.24	99.32	98.46	98.05	95.36	97.20	0.958
RF-6GrVI	91.05	92.40	97.75	89.77	94.26	97.20	93.83	0.907
CART-6GrVI	88.00	90.98	96.87	87.44	92.20	96.33	92.08	0.881
RF-6SeVI	88.86	97.97	92.72	89.94	98.13	91.66	93.26	0.902
CART-6SeVI	87.31	98.02	90.57	87.92	97.60	90.52	92.00	0.880
RF-6PVI	96.30	99.14	98.53	97.56	99.44	97.12	98.03	0.974
CART-6PVI	95.98	98.63	97.21	95.74	98.84	97.26	97.31	0.960
RF-Spring	88.68	94.69	93.43	87.17	97.53	92.15	92.39	0.886
RF-Summer	77.48	91.81	93.02	82.77	94.17	85.91	87.68	0.815
RF-Autumn	70.21	89.46	89.94	76.74	92.40	81.11	83.52	0.752
RF-Winter	73.23	94.15	86.20	79.58	95.91	79.02	84.76	0.771

thresholds determined with training data were 0.224 between *S. alterniflora* and "Others" and 0.529 between *S. alterniflora* and Mangrove trees. Pixels with PNDVI values lower than 0.529 and higher than 0.224 were identified as *S. alterniflora*. For the unsupervised strategy, the thresholds were 0.234 and 0.519, respectively.

Ten-fold validation (see Table III) shows that RF-6PVI approach yielded the highest overall accuracy (98.03%), followed by Supervised Otsu-PNDVI classification algorithm (97.84%). The CART classifier based on 6 PVIs (CART-6PVI) also had a good accuracy (97.31%). The unsupervised Otsu-PNDVI method had 0.64% lower accuracy than supervised Otsu-PNDVI, but the overall accuracy still reached 97.20%. In general, CART produced lower OA than RF classifiers. Besides, with single-season indices such as GrVIs and SeVIs, the overall accuracy is generally low regardless of the classifiers. It is obvious that scene-based ML classification produced much lower accuracies than pixel-based classifications. Although RF-spring yielded 92.39% overall accuracy, both PA and UA of *S. alterniflora* was lower than 89%.

Table IV lists the confusion matrices using 70% reference sample for training and the rest for testing. First, we can conclude that scene-based methods all lead to poorer accuracy compared to other algorithms (OA < 92%). Compared to the supervised Otsu-PNDVI method, the unsupervised Otsu-PNDVI method tended to produce slightly greater confusion between *S. alterniflora* and Mangrove trees, as the threshold determined from the unsupervised Otsu (0.519) was lower than that from the supervised Otsu (0.529). Compared to the ML classification algorithms based on single-season VIs, the thresholding method solely based on PVI has a better performance in distinguishing *S. alterniflora* from its background land cover types. Considerable confusions between *S. alterniflora* and Mangrove trees were produced for the RF-6GrVI and CART-6GrVI algorithms, and confusions between *S. alterniflora* pixels and "Others" were produced for the RF-6SeVI and CART-6SeVI algorithms. It is obvious that the supervised Otsu-PNDVI algorithm has mitigated the confusions better than unsupervised Otsu-PNDVI algorithm.

The Kappa Z-test statistics listed in Fig. 7 demonstrated that while the supervised Otsu-PNDVI-based method did not

statistically improve the accuracy compared to RF and CART classification methods based on the six PVIs, incorporating PVIs in classification, regardless of the classification methods, did improve the accuracy compared to RF and CART classifications using single-season-based VIs. In addition, the Kappa value of the unsupervised Otsu-PNDVI classification was not significantly different from that of the supervised Otsu-PNDVI classification or ML algorithms, indicating that *S. alterniflora* can be detected accurately with PNDVI without the assistance of training datasets. It can be seen that scene-based algorithm has significantly lower accuracy than Otsu-PNDVI-based method.

C. Classification Results

Figs. 8 and 9 show the mapping results of *S. alterniflora* in the three study regions during 2018–2019 with the proposed supervised Otsu-PNDVI method. Table V showcased the detailed distribution area of *S. alterniflora*. The invasive area is 1159.21 ha in Beibu Gulf [see Fig. 8(a)], 245.89 ha in Zhangjiang Estuary [see Fig. 9(a)], and 524.23 ha in Jiulongjiang River Estuary [see Fig. 9(b)]. Note that our observed invasion in Zhangjiang Estuary approximately commensurate with the detection conducted by Tian *et al.* [33], who measured that the invasive area was 270.3 ha by the November 23rd of 2018.

V. DISCUSSION

A. Advantages of PNDVI

This study presented a novel vegetation index that captures the phenological characteristics based on seasonal vegetation indices for invasive plant species identification using pixel-based approach. Previous research has used stacking of multitemporal cloud-free scenes for *S. alterniflora* mapping. For example, Liu *et al.* [36] mapped *S. alterniflora* in Jiangsu Province, East China, using Maxent algorithm based on monthly cloud-free Landsat imagery. However, this scene-based method is not feasible in regions such as our study area because the coastal area in South China was dominated by humid and cloudy weather. For pixel-based approach, pixels across all available Sentinel-2 imagery can be utilized as long as they were not covered by

TABLE IV
CONFUSION MATRIX OF THE SIX CLASSIFICATION METHODS

Reference	Class							
	Others	*S. alterniflora*	Mangrove	PA (%)	Others	*S. alterniflora*	Mangrove	PA (%)
	Supervised OTSU-PNDVI				Unsupervised OTSU-PNDVI			
Others	606	3	0	99.51	607	2	0	99.67
S. alterniflora	17	537	8	95.55	30	518	14	92.17
Mangrove	0	5	593	99.16	0	3	595	99.50
UA (%)	97.27	98.53	98.67	OA (%)=98.13 Kappa=0.972	95.29	99.04	97.70	OA (%)=97.23 Kappa=0.958
	RF-6GrVI				CART-6GrVI			
Others	604	10	0	98.37	592	22	0	96.42
S. alterniflora	19	507	36	90.21	21	491	50	87.37
Mangrove	0	54	544	90.97	1	50	547	91.47
UA (%)	96.95	88.79	93.80	OA(%)=93.29 Kappa=0.899	96.42	87.21	91.62	OA(%)=91.88 Kappa=0.878
	RF-6SeVI				CART-6SeVI			
Others	582	32	0	94.79	562	52	0	91.53
S. alterniflora	71	480	11	85.41	71	477	14	84.88
Mangrove	0	14	584	97.66	2	9	587	98.16
UA (%)	89.13	91.25	98.15	OA(%)=92.78 Kappa=0.892	88.50	88.66	97.67	OA(%)=91.66 Kappa=0.875
	RF-6PVI				CART-6PVI			
Others	607	7	0	98.86	593	21	0	96.58
S. alterniflora	21	537	4	95.55	15	538	9	95.73
Mangrove	0	2	596	99.67	0	2	596	99.67
UA (%)	96.66	98.35	99.33	OA(%)=98.08 Kappa=0.971	97.53	95.90	98.51	OA(%)=97.35 Kappa=0.960
	RF-spring				RF-summer			
Others	503	91	9	91.07	539	73	2	91.88
S. alterniflora	80	414	56	77.48	81	418	63	87.94
Mangrove	10	54	514	89.63	4	46	548	94.65
UA (%)	93.34	79.02	85.90	OA(%)=82.67 Kappa=0.740	93.09	85.81	95.61	OA(%)=84.83 Kappa=0.772
	RF-Autumn				RF-Winter			
Others	542	71	1	87.50	503	105	6	76.14
S.alterniflora	54	481	28	82.80	98	428	36	74.65
Mangrove	1	38	559	96.49	10	33	555	96.15
UA (%)	88.22	82.80	95.69	OA(%)=89.18 Kappa=0.838	79.36	71.36	96.31	OA(%)=83.77 Kappa=0.756

TABLE V
SUMMARY OF CLASSIFICATION OUTCOMES OF THREE GIVEN STUDY SITES

Study sites	AREA (HA)
Beibu Gulf	1159.21
Zhangjiang Estuary	245.89
Jiulongjiang river Estuary	524.23

cloud, so that the cloud-contaminated scenes were fully used. The pixel-based image (or VI) composition strategy might be the only viable solution for vegetation mapping in cloudy regions. It is worth noting that our pixel-based composition strategy was not affected by the inaccuracies in cloud/cirrus masks provided by Sentinel-2 data because the SeVIs and GrVIs extracted the maximum value from the datasets. This also ensures the reliability of the results.

Using the pixel-based composition method, the GrVIs represent the greenest status of a pixel throughout a year, thus, GrVIs performed well in separating vegetation from nonvegetation (see Figs. 4 and 5). However, GrVIs were not preferable in separating *S. alterniflora* from Mangrove trees as they were both large in their growing period in summer season. SeVIs, on the other hand, represent the greenest state of a pixel in senescence season.

The SeVIs of Mangrove trees did not vary significantly from GrVIs as Mangrove trees are evergreen; SeVIs of nonvegetative cover did not vary either, while those of *S. alterniflora* decreased considerably. PVIs neutralized the greenest states in both green and senescence seasons. For Mangrove trees and "Others," PVIs were similar as GrVIs and SeVIs; In contrast, for *S. alterniflora* PVIs were lower than GrVIs but higher than SeVIs. Therefore, PVIs combine the advantage of GrVIs and SeVIs and increase the interclass separability between *S. alterniflora* and non-*S. alterniflora*.

Compared to other PVIs, PNDVI proved to be the most effective one in terms of separability assessment (see Figs. 4 and 5). Interestingly, EVI, which has been well recognized to be an improved version of NDVI, did not show higher interclass variability than NDVI regardless of the seasonal composite. Compared to NDVI, EVI reduces the saturation effect in area with dense vegetation cover. In our study, we also found that both *S. alterniflora* and Mangrove trees had wider range of EVI values (0.1–1 for GrEVI of *S. alterniflora* and 0.36–1 for GrEVI of Mangrove trees) than NDVI values. Therefore, it is inevitable that the resultant PEVI values had greater overlaps.

Previous research has utilized pixel-based composition of time series remotely sensed imagery for vegetation mapping.
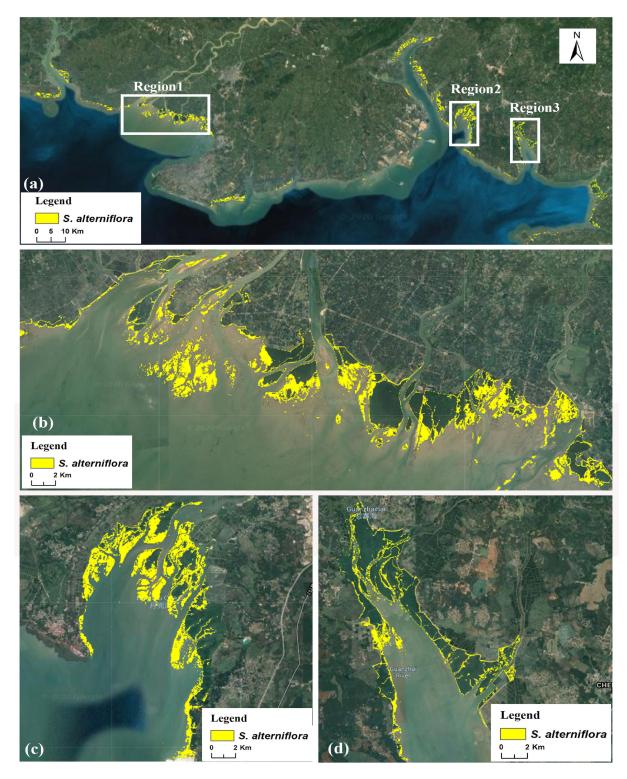
Fig. 8. *S. alterniflora* maps in (a) Beibu Gulf, (b) zoomed-in area of Region 1, (c) zoomed-in area of Region 2, and (d) zoomed-in area of Region 3.

For example, Tian *et al.* [25] composed two 6-band Landsat imageries using cloud-free pixels that have maximum EVI value and using pixels that have maximum plant senescence reflectance index for *S. alterniflora* detection, respectively. Li *et al.* [34] constructed time series Sentinel-2 imagery using harmonic analysis of time series algorithm at pixel level for Mangrove tree species mapping. Karasiak *et al.* [49] constructed time series Formosat-2 imagery by filling cloudy pixels using temporal linear interpolation and conducted forest tree species classification. Most of the existing studies relied on stacking of composited imagery for vegetation classification. In comparison, the PNDVI proposed in our study was simple but effective. Our results showed that *S. alterniflora* can be accurately detected solely based on the PNDVI.

Fig. 9. *S. alterniflora* maps in (a) Zhangjiang Estuary, and (b) Jiulongjiang Estuary.

B. Comparison With ML-Based Classification Methods

Current studies on invasive plant species mapping were dominated by ML classification methods. The general procedures of ML-based classification consist of the following:

1) extracting spectral, spatial, and/or phenological features based on one or more images;
2) using training datasets to establish ML classifiers; and
3) implementing the trained classifiers to classify land cover and vegetation types and extract the target species.

Generally, ML classification methods require large numbers of features, such as spectral features, texture features, and geometric features. For example, Tian *et al.* [33] detected submerged *S. alterniflora* in Zhangjiang Estuary, China, using the RF method based on a total of 35 spectral, geometry, and texture features from Sentinel-2 imagery; the resultant mapping accuracy was over 90%. Tian *et al.* [25] utilized Stacked Auto Encoder to detect *S. alterniflora* based on 12 spectral features composited by imageries at different seasons, and reported 96.22% overall accuracy; the study also reported that the classification accuracy dropped to 83.3% when only summer pixels were used. In addition, parameters in the ML classifiers are subject to adjustment, and inappropriate parameters may degrade the classification accuracies [50]. Furthermore, the choice of classifier is also an influencing factor, as different classifiers may affect the accuracy. In our study, we found that the RF classifiers achieved higher accuracies than CART.

Compared to the more complex ML classification results, both supervised and unsupervised Otsu thresholding approaches solely based on the PNDVI index yielded considerably competitive performances. Besides, the Otsu thresholding approach is more computationally efficient. The unsupervised Otsu thresholding approach produced statistically similar accuracy as the supervised Otsu thresholding approach. Compared to the supervised classification methods, the unsupervised Otsu thresholding method does not require collecting training samples, which might be the most labor intensive and time-consuming task in classification procedures. This is particularly useful for *S. alterniflora* detection over large region such as the South China coastal area.

The high accuracies of the proposed method can be mainly explained by the high spatial and temporal resolution of Sentinel-2 imagery, the utilization of pixel-based composition strategy and good separability of PNDVI. The 10 m spatial resolution allows us to detect small vegetation patches, which are not possible for Landsat-series imagery. With 5-day revisiting cycle, the time series Sentinel-2 observations could capture the greenest state of a pixel in both green period and senescence period with the assistance of pixel-based composition strategy.

C. Opportunities and Challenges

In this study, we demonstrated that the PNDVI-based Otsu thresholding methods (supervised or unsupervised) proposed in our study were simple, efficiently applicable for *S. alterniflora* mapping in South China coastal region. The PNDVI enhanced the separability between *S. alterniflora* and non-*S. alterniflora* by considering the differences in phenological characteristics of vegetation types in the study areas. The Otsu thresholding method was easy to implement, indicating that it could be widely accepted by coastal wetland managers. Because each vegetation type has its own growth rhythm and phenological characteristics, the perspective of pixel-based phenological index construction can be utilized for other vegetation mapping tasks.

It should be noted that the success of PNDVI in our study were mainly dependent on the distinct phenological difference

of *S. alterniflora* and Mangrove trees. In the coastal wetlands where strong phenological contrast between *S. alterniflora* and native plants species were not available, PNDVI might lead to poorer accuracies. However, this problem can be overcome by carefully examining the phenological features of each vegetation types before classification. For example, in the Yellow River delta in North China, *S. alterniflora* and the native Phragmites Australis have one month differences in the start of growing season and end of growing season [51]. It is possible to utilize the time window for the construction of PVI. Time window was also proved important as in a recent study by Zhang *et al.* [27], which examined differences in time series spectral indices of *S. alterniflora* and other vegetation species in Chongming island in Eastern China, and found that using land surface water index during April–May was most effective in extraction of *S. alterniflora*. Sun *et al.* [22] found that April, May, and November are important months for classifying salt marsh at species level. However, when time window is too narrow, it is possible that the number of valid observations is insufficient to derive VIs for each pixel.

Our results proved the promising potential of time series Sentinel-2 data for *S. alterniflora* mapping in cloudy South China due to its high temporal frequency. Before Sentinel-2 A/B constellation began to provide 5-day revisiting imagery in March 2017, the combined use of Landsat 7 ETM+ and Landsat 8 OLI (or Landsat 7 ETM+ and Landsat 5 TM before 2012) might also be used to map *S. alterniflora* as they could provide 8-day revisiting period.

VI. CONCLUSION

In this study, we proposed a new vegetation index, namely PNDVI for detection and mapping of invasive species, *S. alterniflora*, using Sentinel-2 data with the assistance of GEE platform. Taking South China coastal regions as study areas, our results showed that the PNDVI enhanced the separability between *S. alterniflora* and non-*S. alterniflora* land cover types compared to single-season-based VIs, as well as other 5 PVIs. Based on the PNDVI values, Otsu thresholding algorithm was applied with or without training datasets. Ten-fold cross validation showed that the supervised Otsu-PNDVI method yielded high classification accuracy for discriminating *S. alterniflora* (OA = 97.84%, Kappa = 0.968). Kappa Z-statistical test suggested that the Otsu-PNDVI method yielded similar accuracy as RF-6PVI. However, compared to ML-based algorithms, this method is simpler and more efficient as it only requires one feature. In addition, the unsupervised Otsu-PNDVI method produced comparable accuracies to the supervised Otsu-PNDVI and ML-based algorithm. The pixel-based Otsu-PNDVI method showed superior performance over scene-based method. As collecting training samples were probably the most time consuming and labor-intensive task in supervised classification procedures, the success of unsupervised Otsu-PNDVI method suggests that the method is more practical, operational and has potential to be widely implemented in areas such as South China coast. It is also anticipated that PNDVI has the opportunity of bringing assistance for uncovering the invasive mechanism as well as giving aid for planning protection to potentially hazardous regions.

REFERENCES

[1] D. R. Strong and D. R. Ayres, "Ecological and evolutionary misadventures of Spartina," *Annu. Rev. Ecol., Evol., Systematics*, vol. 44, pp. 389–410, 2013.
[2] A. S. Vaz, D. Alcaraz-Segura, J. C. Campos, J. R. Vicente, and J. P. Honrado, "Managing plant invasions through the lens of remote sensing: A review of progress and the way forward," *Sci. Total Environ.*, vol. 642, pp. 1328–1339, 2018.
[3] B. Ge, S. Jiang, L. Yang, H. Zhang, and B. Tang, "Succession of macro-faunal communities and environmental properties along a gradient of smooth cordgrass Spartina alterniflora invasion stages," *Mar. Environ. Res.*, vol. 156, 2020, Art. no. 104862.
[4] M. L. Aïnouche *et al.*, "Hybridization, polyploidy and invasion: Lessons from Spartina (Poaceae)," *Biol. Invasions*, vol. 11, no. 5, 2009, Art. no. 1159.
[5] B.-S. Cui, Q. He, and Y. An, "Spartina alterniflora invasions and effects on crab communities in a western Pacific estuary," *Ecol. Eng.*, vol. 37, no. 11, pp. 1920–1924, 2011.
[6] R.-M. Yang, "Characterization of the salt marsh soils and visible-near-infrared spectroscopy along a chronosequence of Spartina alterniflora invasion in a coastal wetland of eastern China," *Geoderma*, vol. 362, 2020, Art. no. 114138.
[7] N. Li, L. Li, Y. Zhang, and M. Wu, "Monitoring of the invasion of Spartina alterniflora from 1985 to 2015 in Zhejiang Province, China," *BMC Ecol.*, vol. 20, no. 1, pp. 1–12, 2020.
[8] J. Lu and Y. Zhang, "Spatial distribution of an invasive plant Spartina alterniflora and its potential as biofuels in China," *Ecol. Eng.*, vol. 52, pp. 175–181, 2013.
[9] D. Mao *et al.*, "Rapid invasion of Spartina Alterniflora in the coastal zone of mainland China: Spatiotemporal patterns and human prevention," *Sensors*, vol. 19, no. 10, 2019, Art. no. 2308.
[10] Q. Wang *et al.*, "Effects of growing conditions on the growth of and interactions between salt marsh plants: Implications for invasibility of habitats," *Biol. Invasions*, vol. 8, no. 7, pp. 1547–1560, 2006.
[11] Q. Wang, S. Q. An, Z. J. Ma, B. Zhao, and L. Bo, "Invasive Spartina alterniflora: Biology, ecology and management," *Acta Phytotaxonomica Sinica*, vol. 44, no. 5, pp. 559–588, 2006.
[12] J. Tian *et al.*, "Comparison of UAV and WorldView-2 imagery for mapping leaf area index of Mangrove forest," *Int. J. Appl. Earth Observ. Geoinf.*, vol. 61, pp. 22–31, 2017.
[13] Y. Zhang, G. Huang, W. Wang, L. Chen, and G. Lin, "Interactions between mangroves and exotic Spartina in an anthropogenically disturbed estuary in southern China," *Ecology*, vol. 93, no. 3, pp. 588–597, 2012.
[14] Y. Zhang, S. C. Pennings, B. Li, and J. J. E. Wu, "Biotic homogenization of wetland nematode communities by exotic Spartina alterniflora in China," *Ecology*, vol. 100, no. 4, 2019, Art. no. e02596.
[15] C. Zhou *et al.*, "Sulfur storage changed by exotic Spartina alterniflora in coastal saltmarshes of China," *Ecol. Eng.*, vol. 35, no. 4, pp. 536–543, 2009.
[16] P. Zuo, S. Zhao, C. A. Liu, C. Wang, and Y. Liang, "Distribution of Spartina spp. along China's coast," *Ecol. Eng.*, vol. 40, pp. 160–166, 2012.
[17] F. Alvarez-Taboada, C. Paredes, and J. Julián-Pelaz, "Mapping of the invasive species Hakea sericea using unmanned aerial vehicle (UAV) and WorldView-2 imagery and an object-oriented approach," *Remote Sens.*, vol. 9, no. 9, 2017, Art. no. 913.
[18] J. Müllerová, T. Bartaloš, J. Brůna, P. Dvořák, and M. Vítková, "Unmanned aircraft in nature conservation: An example from plant invasions," *Int. J. Remote Sens.*, vol. 38, no. 8–10, pp. 2177–2198, 2017.
[19] K. Peerbhay, O. Mutanga, R. Lottering, and R. Ismail, "Mapping Solanum mauritianum plant invasions using WorldView-2 imagery and unsupervised random forests," *Remote Sens. Environ.*, vol. 182, pp. 39–48, 2016.
[20] C. Diao and L. Wang, "Incorporating plant phenological trajectory in exotic saltcedar detection with monthly time series of Landsat imagery," *Remote Sens. Environ.*, vol. 182, pp. 60–71, 2016.
[21] M. Liu *et al.*, "Monitoring the invasion of Spartina alterniflora using multi-source high-resolution imagery in the Zhangjiang Estuary, China," *Remote Sens.*, vol. 9, no. 6, 2017, Art. no. 539.

[22] C. Sun, Y. Liu, S. Zhao, M. Zhou, Y. Yang, and F. Li, "Classification mapping and species identification of salt marshes based on a short-time interval NDVI time-series from HJ-1 optical imagery," *Int. J. Appl. Earth Observ. Geoinf.*, vol. 45, pp. 27–41, 2016.

[23] J. Wang *et al.*, "Mapping the dynamics of eastern redcedar encroachment into grasslands during 1984–2010 through PALSAR and time series Landsat images," *Remote Sens. Environ.*, vol. 190, pp. 233–246, 2017.

[24] X. Zhu, L. Meng, Y. Zhang, Q. Weng, and J. Morris, "Tidal and meteorological influences on the growth of invasive *Spartina alterniflora*: Evidence from UAV remote sensing," *Remote Sens.* vol. 11, no. 10, 2019, Art. no. 1208.

[25] J. Tian *et al.*, "Development of spectral-phenological features for deep learning to understand *Spartina alterniflora* invasion," *Remote Sens. Environ.*, vol. 242, 2020, Art. no. 111745.

[26] P. Griffiths, S. van der Linden, T. Kuemmerle, and P. Hostert, "A pixel-based Landsat compositing algorithm for large area land cover mapping," *IEEE J. Sel. Topics Appl. Earth Observ. Remote Sens.*, vol. 6, no. 5, pp. 2088–2101, Oct. 2013.

[27] X. Zhang *et al.*, "Quantifying expansion and removal of *Spartina alterniflora* on Chongming island, China, using time series Landsat images during 1995–2018," *Remote Sens. Environ.*, vol. 247, 2020, Art. no. 111916.

[28] R. Bost, R. A. Popa, S. Tu, and S. Goldwasser, "Machine learning classification over encrypted data," in *Proc. Netw. Distrib. Syst. Secur. Symp.*, 2015, Art. no. 4325.

[29] S. M. Weiss and I. Kapouleas, "An empirical comparison of pattern recognition, neural nets, and machine learning classification methods," in *Proc. Int. Joint Conf. Artif. Intell.*, 1989, pp. 781–787.

[30] A. Wang *et al.*, "Monitoring the invasion of *Spartina alterniflora* from 1993 to 2014 with Landsat TM and SPOT 6 satellite data in Yueqing Bay, China," *PLoS One*, vol. 10, no. 8, 2015, Art. no. e0135538.

[31] W. Lin, G. Chen, P. Guo, W. Zhu, and D. Zhang, "Remote-sensed monitoring of dominant plant species distribution and dynamics at Jiuduansha Wetland in Shanghai, China," *Remote Sens.*, vol. 7, no. 8, pp. 10227–10241, 2015.

[32] R. Piiroinen, F. E. Fassnacht, J. Heiskanen, E. Maeda, B. Mack, and P. Pellikka, "Invasive tree species detection in the Eastern Arc Mountains biodiversity hotspot using one class classification," *Remote Sens. Environ.*, vol. 218, pp. 119–131, 2018.

[33] Y. Tian, M. Jia, Z. Wang, D. Mao, B. Du, and C. Wang, "Monitoring invasion process of *Spartina alterniflora* by seasonal Sentinel-2 imagery and an object-based random forest classification," *Remote Sens.*, vol. 12, no. 9, 2020, Art. no. 1383.

[34] H. Li, M. Jia, R. Zhang, Y. Ren, and X. Wen, "Incorporating the plant phenological trajectory into mangrove species mapping with dense time series Sentinel-2 imagery and the Google Earth Engine platform," *Remote Sens.*, vol. 11, no. 21, 2019, Art. no. 2479.

[35] D. Wang, W. Huang, R. Liang, and F. Li, "Effects of *Spartina alterniflora* invasion on soil quality in coastal wetland of Beibu Gulf of South China," *Plos One*, vol. 11, no. 12, 2016, Art. no. e0168951.

[36] X. Liu, H. Liu, H. Gong, Z. Lin, and S. Lv, "Appling the one-class classification method of Maxent to detect an invasive plant *Spartina alterniflora* with time-series analysis," *Remote Sens.*, vol. 9, no. 11, 2017, Art. no. 1120.

[37] C. J. Tucker, "Red and photographic infrared linear combinations for monitoring vegetation," *Remote Sens. Environ.*, vol. 8, pp. 127–150, 1978.

[38] A. Huete, K. Didan, T. Miura, E. P. Rodriguez, X. Gao, and L. G. Ferreira, "Overview of the radiometric and biophysical performance of the MODIS vegetation indices," *Remote Sens. Environ.*, vol. 83, no. 1/2, pp. 195–213, 2002.

[39] C. F. Jordan, "Derivation of leaf-area index from quality of light on the forest floor," *Ecology*, vol. 50, no. 4, pp. 663–666, 1969.

[40] R. P. Sripada, R. W. Heiniger, J. G. White, and A. D. Meijer, "Aerial color infrared photography for determining early in-season nitrogen requirements in corn," *Agronomy J.*, vol. 98, no. 4, pp. 968–977, 2006.

[41] A. A. Gitelson and M. N. Merzlyak, "Remote sensing of chlorophyll concentration in higher plant leaves," *Adv. Space Res.*, vol. 22, no. 5, pp. 689–692, 1998.

[42] A. R. Huete, "A soil-adjusted vegetation index (SAVI)," *Remote Sens. Environ.*, vol. 25, pp. 295–309, 1988.

[43] Z. T. Ouyang, Y. Gao, X. Xie, H. Q. Guo, T. T. Zhang, and B. Zhao, "Spectral discrimination of the invasive plant spartina alterniflora at multiple phenological stages in a Saltmarsh Wetland," *PLoS One*, vol. 8, no. 6, 2013, Art. no. e67315.
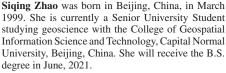
[44] J. Ai, W. Gao, Z. Gao, R. Shi, and C. Zhang, "Phenology-based *Spartina alterniflora* mapping in coastal wetland of the Yangtze Estuary using time series of GaoFen satellite no. 1 wide field of view imagery," *J. Appl. Remote Sens.*, vol. 11, no. 2, 2017, Art. no. 026020.

[45] B. Somers, S. Delalieux, W. Verstraeten, J. Van Aardt, G. Albrigo, and P. Coppin, "An automated waveband selection technique for optimized hyperspectral mixture analysis," *Int. J. Remote Sens.*, vol. 31, no. 20, pp. 5549–5568, 2010.

[46] N. Otsu, "A threshold selection method from gray-level histograms," *IEEE Trans. Syst., Man, Cybern.*, vol. SMC-9, no. 1, pp. 62–66, Jan. 1979.

[47] Y. Ke, L. J. Quackenbush, and J. Im, "Synergistic use of quickbird multispectral imagery and LIDAR data for object-based forest," *Remote Sens. Environ.*, vol. 114, pp. 1141–1154, 2010.

[48] R. G. Congalton and K. Green, *Assessing the Accuracy of Remotely Sensed Data: Principles and Practices.* Cleveland, OH, USA: CRC Press, 2019, pp. 105–110.

[49] N. Karasiak, J.-F. Dejoux, M. Fauvel, J. Willm, C. Monteil, and D. Sheeren, "Statistical stability and spatial instability in mapping forest tree species by comparing 9 years of satellite image time series," *Remote Sens.*, vol. 11, no. 21, 2019, Art. no. 2512.

[50] T. Abeysinghe, "Mapping invasive phragmites australis in the old woman creek estuary using UAV remote sensing and machine learning classifiers," *Remote Sens.*, vol. 11, no. 11, 2019, Art. no. 1380.

[51] G.-B. Ren *et al.*, "Monitoring the invasion of smooth cordgrass spartina alterniflora within the modern yellow river delta using remote sensing," *J. Coastal Res.*, vol. 90, no. sp1, pp. 135–145, 2019.

Ronglong Xu was born in Fujian, China, in June 1999. He is currently a Senior University Student studying remote sensing with the College of Geospatial Information Science and Technology, Capital Normal University, Beijing, China. He will receive the B.S. degree in remote sensing, in June 2021.

His research interests include ecological remote sensing and environmental resource detection, especially related to phenological vegetation identification and detection.

Siqing Zhao was born in Beijing, China, in March 1999. She is currently a Senior University Student studying geoscience with the College of Geospatial Information Science and Technology, Capital Normal University, Beijing, China. She will receive the B.S. degree in June, 2021.

Her research interests include the ecological remote sensing and global changes, especially invasive species detection.

Yinghai Ke received the B.S. degree in environmental science from Wuhan University, Wuhan, China, in 2002, the M.Sc. degree from the Peking University, Beijing, China, in 2005, and the Ph.D. degree from State University of New York College of Environmental Science and Forestry (SUNY ESF), Syracuse, NY, USA, in 2009.

Since 2010, she has been with the Hydrology Group, Pacific Northwest National Laboratory, Richland, WA, USA, as a Research Scientist. She has become an Associate Professor with Capital Normal University, Beijing, China, since 2013. Her research interests include remote sensing application in ecohydrology.